Hindawi
Journal of Sensors
Volume 2021, Article ID 8875907, 9 pages
https://doi.org/10.1155/2021/8875907

Research Article

A Wireless Passive Vibration Sensor Based on High-Temperature Ceramic for Harsh Environment

Chen Li,[1,2] Yanan Xue,[1,2] Pengyu Jia,[1] Mangu Jia,[1] Boshan Sun,[1,2] and Jijun Xiong[1,2]

[1]*Science and Technology on Electronic Test and Measurement Laboratory, Taiyuan 030051, China*
[2]*Key Laboratory of Instrumentation Science and Dynamic Measurement, Ministry of Education, North University of China, Taiyuan 030051, China*

Correspondence should be addressed to Jijun Xiong; xiongjijun@nuc.edu.cn

Received 26 September 2020; Revised 8 November 2020; Accepted 12 December 2020; Published 12 January 2021

Academic Editor: Praveen K. Sekhar

This paper proposes a wireless passive vibration sensor based on high-temperature ceramics for vibration measurement in harsh environments such as automotive and advanced engines. The sensor can be equivalent to an acceleration-sensitive RF LC resonance tank. The structural design of the LC tank and the signal wireless sensing mechanism are introduced in detail. The high-temperature mechanical properties of the sensitive structure are analyzed using ANSYS at 25–400°C, which proves the usability of the vibration sensor in high-temperature environment. The three-dimensional integrated manufacturing of vibration sensors with a beam-mass structure based on high-temperature ceramics is completed by a bonding process. Finally, the performance of the sensor is tested on a built experimental platform, and the results show that the vibration sensitivity is approximately 1.303 mv/m·s^{-2}, and the nonlinear error is approximately 4.3%. The vibration sensor can work normally within 250°C, and the sensitivity is 0.989 mv/m·s^{-2}.

1. Introduction

In aviation, automobiles, and other fields, the monitoring of vibration parameters is critically essential to the normal operation of key components of certain large-scale facilities and equipment [1–4]. For example, the aero-engine under working conditions is usually accompanied by severe vibrations, which has a great impact on the life span of components and even causes accidents in serious cases [5]. Therefore, the real-time measurement of vibration parameters has become crucial for prolonging the life span and improving the reliability of the system. At present, various vibration sensors based on different sensitive principles such as piezoresistive, piezoelectric, and capacitive have been known and used for vibration measurement. For example, in [6], a quad beam piezoresistive z-axis accelerometer with silicon as material was presented, which relied on the piezoresistive effect to measure the acceleration. In [7], an X-shaped piezoelectric accelerometer was proposed, which detected acceleration signal by sticking PZT piezoelectric film to the root of silicon sensitive beam. In general, capacitive vibration sensors are designed as differential structure so as to improve sensitivity and reduce nonlinear errors. In [8], a z-axis differential capacitance accelerometer with double-side single crystal silicon H-shape structure was researched, which realized the stable measurement of acceleration with 0-1 g. However, the vibration sensors based on the above-mentioned sensitive mechanisms all use wired measurement methods, which means the sensitive chip and the back-end processing circuit are directly connected by leads, which cannot be used in some specific environments. For example, for the parameter measurement of high-speed rotating parts, when the sensor is installed on the surface of the high-speed rotating part, the electrical lead will move with the rotating device, which will lead to breakage and failure of the test. Thus, the wireless passive LC resonant sensor, which does not rely on interconnection lines to transmit signals and an external power supply to provide energy, and has a simple structure and convenient reading, has attracted wide attention at home and abroad [9–17, 22]. In recent years, acceleration measurement based on this principle has gradually arisen. Wei [18] in 2016 studied the temperature-

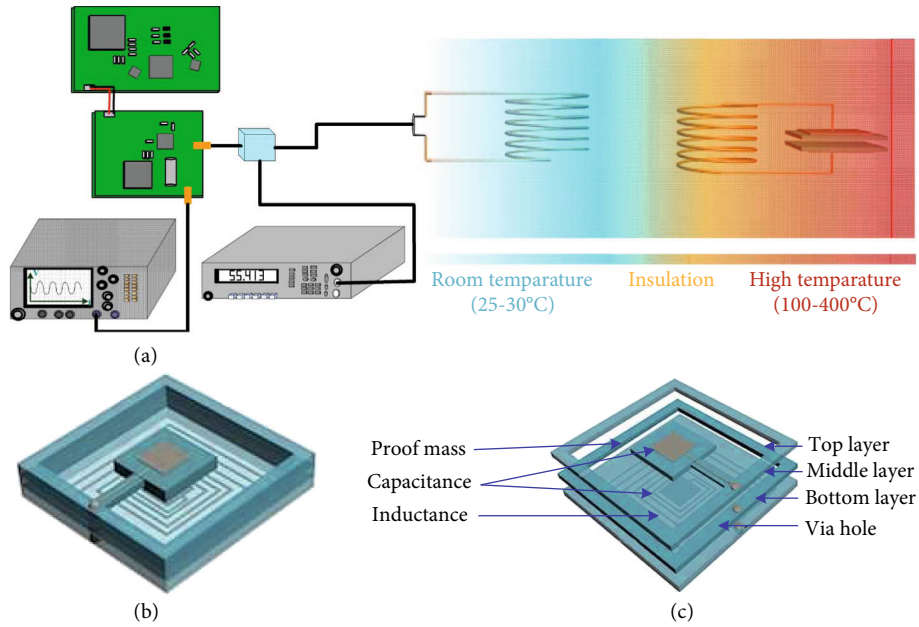

Figure 1: (a) Schematic diagram of the wireless sensing principle; (b) 3D model diagram of vibration sensor; (c) schematic structure of vibration sensor.

pressure-acceleration three-parameter sensor using the LC resonance principle, which mainly focused on structure design and simulation analysis. Liu [19] in 2018 proposed an LTCC (Low Temperature Co-fired Ceramic) capacitive vibration sensor and measured ±1 g acceleration using the dividing head. However, it only aimed at the static measurement of acceleration, which is far from satisfying the real-time measurement of dynamic acceleration signal. In addition, compared with the LTCC materials, the high-temperature ceramic materials can be used in a higher temperature environment owing to the material properties.

In this paper, a wireless passive LC resonant vibration sensor using zirconia ceramic with low elastic modulus as a sensitive material is presented. The sensor consisted of a constant square inductor and variable parallel capacitor, and the movable plate of the capacitor was a beam-mass structure. In addition, wireless transmission of the vibration signal was based on the principle of mutual inductance coupling between the inductor coil and the antenna coil. The mechanical properties of the sensitive beam-mass structure in a high-temperature environment were simulated by ANSYS to verify the usability of the sensor. The integrated preparation of the sensor embedded with the beam-mass structure was completed by a bonding process. Finally, a vibration test platform was built to verify the performance of the fabricated sensor.

2. Measurement Principle and Design of Passive Vibration Sensor

The wireless sensing mechanism of the vibration sensor is shown in Figure 1(a). A constant spiral inductor and a variable parallel capacitor are connected in series to form a vibration sensing circuit, which measures acceleration by detecting the deformation of the movable plate of the capacitor. The capacitance of the capacitor changes due to the acceleration applied on the movable plate of the capacitor, resulting in a change in the equivalent impedance at the antenna. The signal at the antenna is partially reflected due to impedance mismatch, which is input into the detection circuit through the CPL port of the coupler; the voltage signal output by the detection circuit changes accordingly. The value of the constant inductor can be calculated as follows [20]:

$$L_s = 2.34\mu_0 \frac{n^2((d_{\text{out}} + d_{\text{in}})/2)}{1 + 2.75((d_{\text{out}} - d_{\text{in}})/(d_{\text{out}} + d_{\text{in}}))}, \quad (1)$$

where μ_0 is the permeability of vacuum, n is the number of turns of the square spiral inductor coil, and d_{out} and d_{in} are the out diameter and inner diameter of the coil, respectively. Since the vibration parameter is sensed by the beam in this paper, the displacement of beam under acceleration g that can be expressed as:

$$\Delta d = \frac{Fl^3}{3EI} = \frac{4mgl^3}{Ebh^3}, \quad (2)$$

where E is the elastic modulus of zirconia ceramics, F is the inertial force applied to the mass, l, b, and h are the length, width, and height of cantilever beam, respectively, and m is the quality of mass block. The capacitance of the sensor under acceleration g is:

$$C = f(g) = \frac{\varepsilon_0 A}{d_0 + (t_g/\varepsilon_r) - (4mgl^3/Ebh^3)}, \quad (3)$$

where ε_0 is the dielectric constant of vacuum, ε_r is the relative dielectric constant of substrate.A is the facing area

of capacitor plates, d_0 is the initial distance of capacitor plates, and t_g is the thickness of zirconia dielectric layer. The equivalent impedance of the antenna can be represented by [21]:

$$Z_{\text{in}} = f(C) = R_a + j\omega L_a + \frac{\omega_2 M_2}{R_s + j(\omega L_s - (1/\omega C))}, \quad (4)$$

where R_a and R_s, respectively, present the resistance of the antenna and sensor, w is the angular frequency, L_a and L_s, respectively, present the inductance at the antenna and sensor, and C is the equivalent capacitance at the sensor. M presents the mutual inductance between the antenna and the sensor coupled coil, and it is expressed as [22]:

$$M = k\sqrt{L_a L_s}, \quad (5)$$

where k presents the coupling coefficient of the antenna and sensor. According to impedance matching characteristics, the reflection coefficient Γ at the antenna can be expressed as follows:

$$\Gamma = f(Z_{\text{in}}) = \left.\frac{Z_{\text{in}} - Z_0}{Z_{\text{in}} + Z_0}\right|_{Z_0=50\Omega} = 1 - \frac{100}{Z_{\text{in}} + 50}. \quad (6)$$

The reflected signal is converted into voltage by the measuring circuit and output, and its expression is

$$V_{\text{out}} = f(\Gamma) = G_{\text{env}} \cdot C_{31} \cdot \Gamma = G_{\text{env}} \cdot C_{31} \cdot \left(1 - \frac{100}{Z_{\text{in}} + 50}\right), \quad (7)$$

where G_{env} is the amplification gain, and its value is 1.46 and C_{31} is the coupling coefficient between the coupled port and the input port. It can be seen from the above formula that the output voltage of the detection circuit changes with the capacitance, and the change of the capacitance reflects the change of the acceleration. Therefore, the acceleration measurement can be realized by analyzing the value of the output voltage of the circuit.

In this study, high-temperature resistant ceramic materials and conductive silver paste with low resistivity and good adhesion are selected as materials of the vibration sensor. As shown in Figures 1(b) and 1(c), the sensor consists of three layers. The top layer includes a beam-mass structure made of zirconia with low elastic modulus, which is used to print the movable plate of the capacitor. The mass block is fixed to the top frame by the cantilever beam. The middle layer contains a frame layer, which provides some space for the beam to deform under acceleration. The bottom layer is a square solid substrate for printing inductor and capacitor fixed plate. Both the middle and bottom layers are made of alumina ceramics. The area of the capacitor bottom plate is smaller than that of the mass block, which is beneficial for reducing the influence of the edge capacitance.

The sensor is composed of 14 layers of ceramic green tape, and the thickness of each layer of green tape is about 100 μm. The top, middle, and bottom layers contain 2, 2, and 10 layers, respectively. The thickness of the mass block is designed to be twice the thickness of the beam so that the inertial force can be increased under the same acceleration to obtain greater displacement. Table 1 lists the detailed parameters of the designed vibration sensor.

Table 1: Geometric dimensions of the as-designed accelerometer.

Parameter	Symbol	Value
d_{in}	Inner diameter	11 mm
d_{out}	Outer diameter	49 mm
A	Side length of plate	8 mm
d_0	Initial spacing	1.4 mm
l	Length of beam	10 mm
b	Width of beam	3 mm
h	Thickness of beam	100 μm
a	Side of mass	13 mm
h_1	Thickness of mass	200 μm

3. ANSYS Finite Element Simulation of Sensitive Beam-Mass Structure

3.1. Simulation of Mechanical Properties at Room Temperature. According to the geometric dimensions of beam and mass listed in Table 1, ANSYS workbench is used to simulate the mechanical properties of the sensitive structure, and the SolidWorks software is used to model the sensitive structure.

After importing the modeled sensitive beam into ANSYS, a static analysis of the structure is performed. In order to perform finite element simulations, it is necessary to mesh the structure. The quality of the mesh directly affects the solution time and the correctness of the solution result. As shown in Figure 2(a), the minimum mesh quality is 0.7869, which indicates that the divided mesh is suitable. Figure 2(b) shows the equivalent stress distribution of the sensitive beam under a 4 g load. It can be observed that the maximum value is 7.818 MPa, which is found at the fixed position of the sensitive beam and is much smaller than the bending strength of the material. It is proved that the displacement of the beam changes linearly in the range of 4 g.

Modal analysis and harmonious response analysis of cantilever beam are used to characterize its anti-interference ability. After extracting the first two-order vibration modes of the beam, as shown in Figures 3(a) and 3(b), we can see that the frequency of the first-order vibration mode, which is also known as the working mode, is 165.54 Hz; it appears to move along the z-axis of the center of the mass block. The second-order vibration mode is an interference mode with a frequency of 660.81 Hz, which appears to rotate around the x-axis of the center of the mass, and the frequency of the second-order interference mode is more than three times that of the first-order working mode. Figures 3(c) and 3(d) show the harmonic response analysis of the structure,

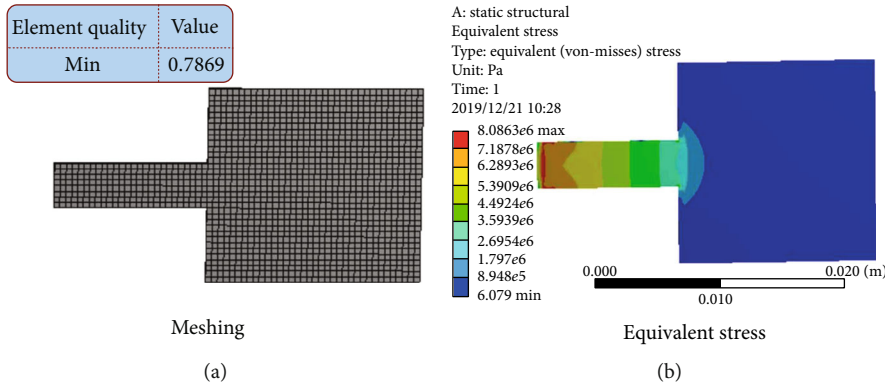

Figure 2: (a) Meshing of sensitive structure; (b) equivalent stress under 4 g.

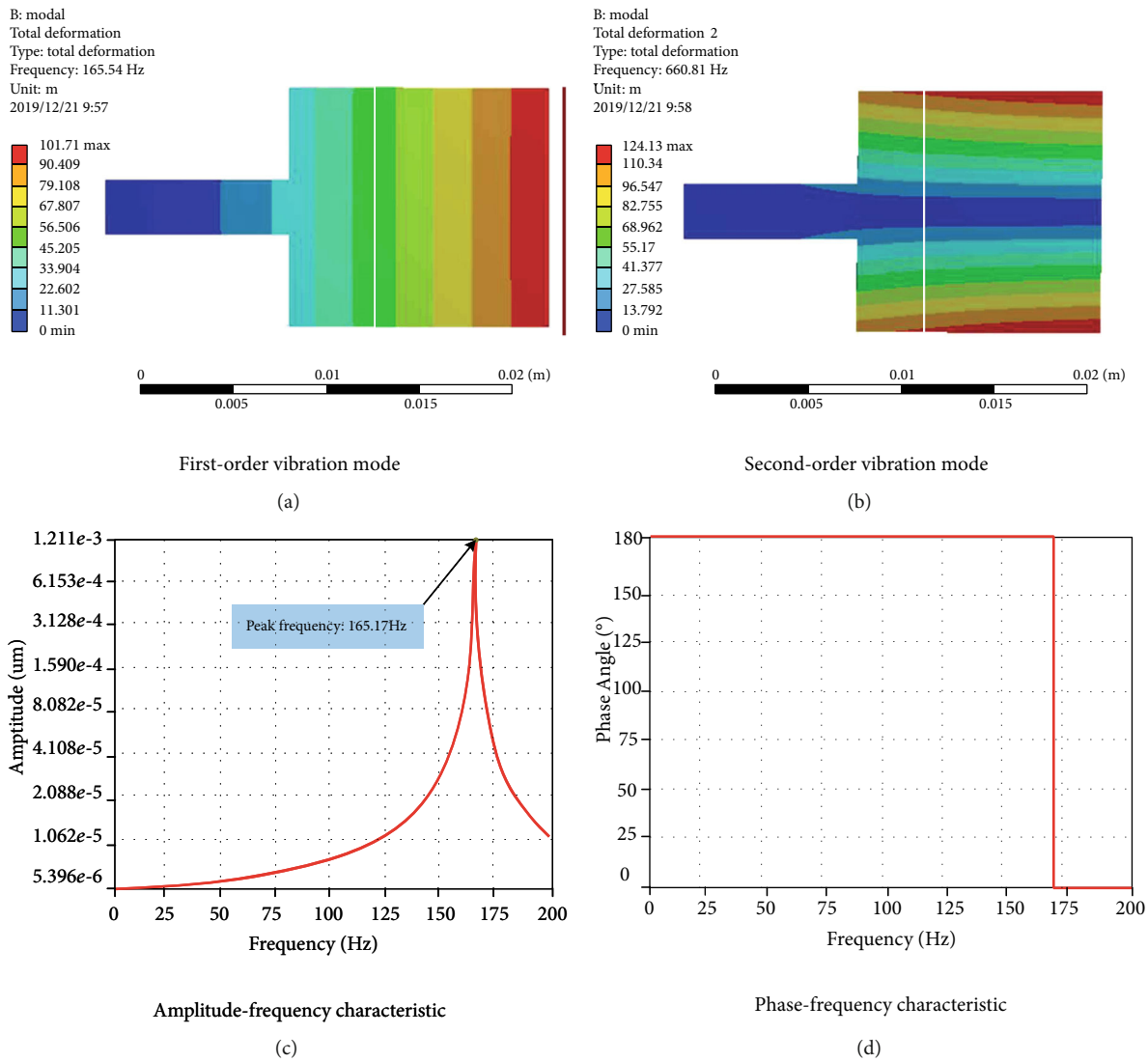

Figure 3: Dynastic characteristic of sensitive beam: (a) first-order vibration mode; (b) second-order vibration mode; (c) amplitude-frequency characteristic; (d) phase-frequency characteristic.

which represent amplitude-frequency characteristics and phase-frequency characteristics, respectively. The peak frequency is 165.17 Hz, which is almost the same as the frequency of the first-order vibration mode. The results of the above dynamic analyses show that the sensitive structure has strong anti-interference ability.

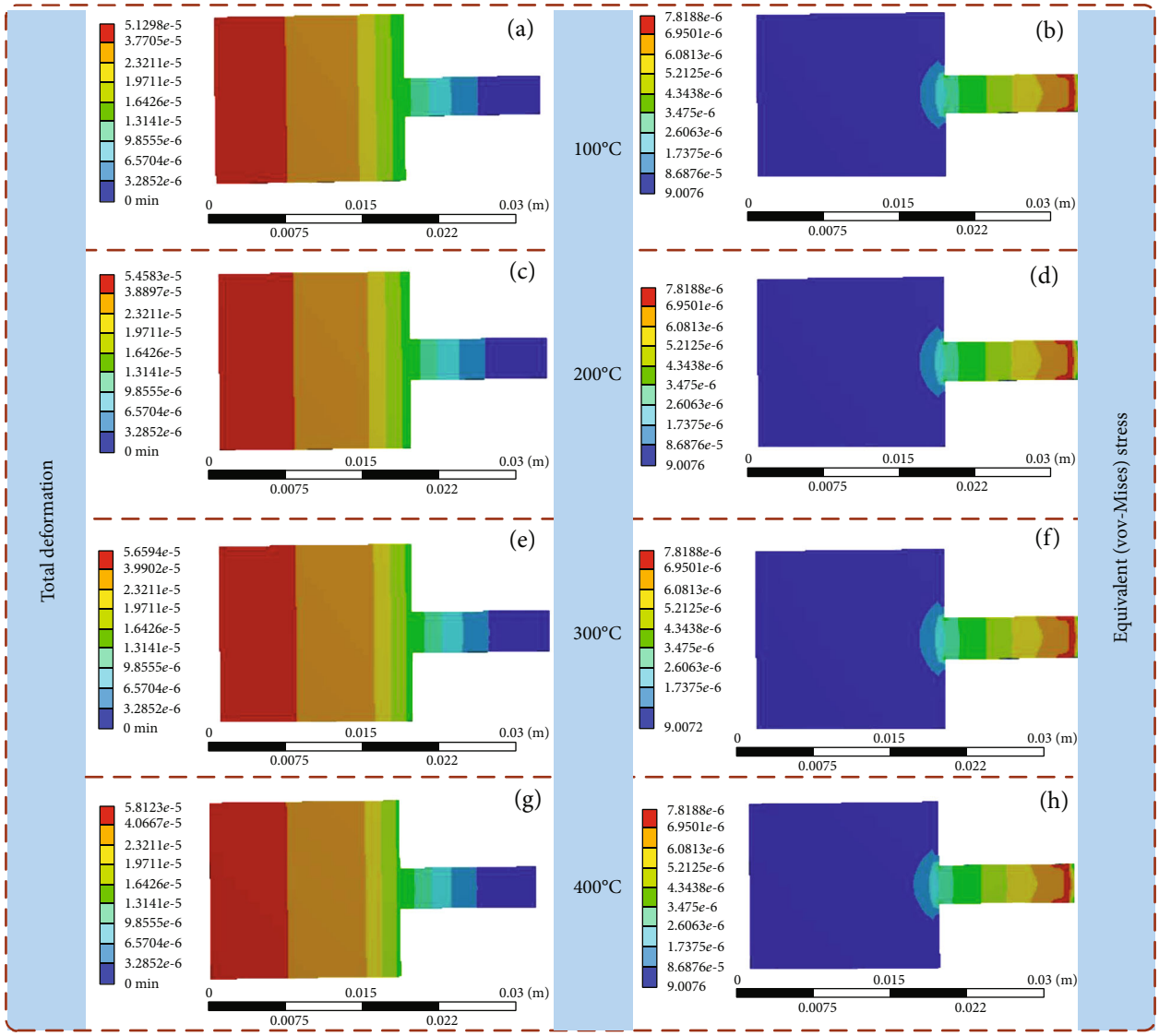

FIGURE 4: Static characteristics in the z-axis direction at different temperatures: (a) deformation distribution of sensitive beam at 100°C; (b) equivalent stress distribution of sensitive beam at 100°C; (c) deformation distribution of sensitive beam at 200°C; (d) equivalent stress distribution of sensitive beam at 200°C; (e) deformation distribution of sensitive beam at 300°C; (f) equivalent stress distribution of sensitive beam at 300°C; (g) deformation distribution of sensitive beam at 400°C; (h) equivalent stress distribution of sensitive beam at 400°C.

3.2. Simulation of Mechanical Properties at High-Temperature Environment. As the temperature increases, the mechanical parameters of the sensitive beam will change, thereby changing the performance of the sensor. Therefore, this section simulates the mechanical properties in the temperature-acceleration coupled field. In order to simplify the model, the internal thermal stress of the material is ignored, and the structure is assumed to be heated uniformly. Under 4 g acceleration, the temperature load applied to the sensitive beam changes from 100°C to 400°C, and the results are shown in Figure 4. It can be observed that the deflection of the sensitive beam increases with an increase in temperature, which is mainly because the elastic modulus of the zirconia material decreases with an increase in temperature. The maximum equivalent stress of the sensitive beam does not change with temperature, and it can be expressed as:

$$\sigma = \frac{6mal}{bh^2}. \tag{8}$$

We can see from Equation (8) that the maximum stress of the cantilever beam is only related to the structure size and has nothing to do with the elastic modulus. The flexural strength of zirconia at 400°C is approximately 600 MPa. After considering a safety factor, its maximum allowable stress should be greater than 400 MPa. The simulation results show that the equivalent stress under 4 g load is 7.8188 MPa, which is much smaller than the maximum allowable stress. Therefore, the

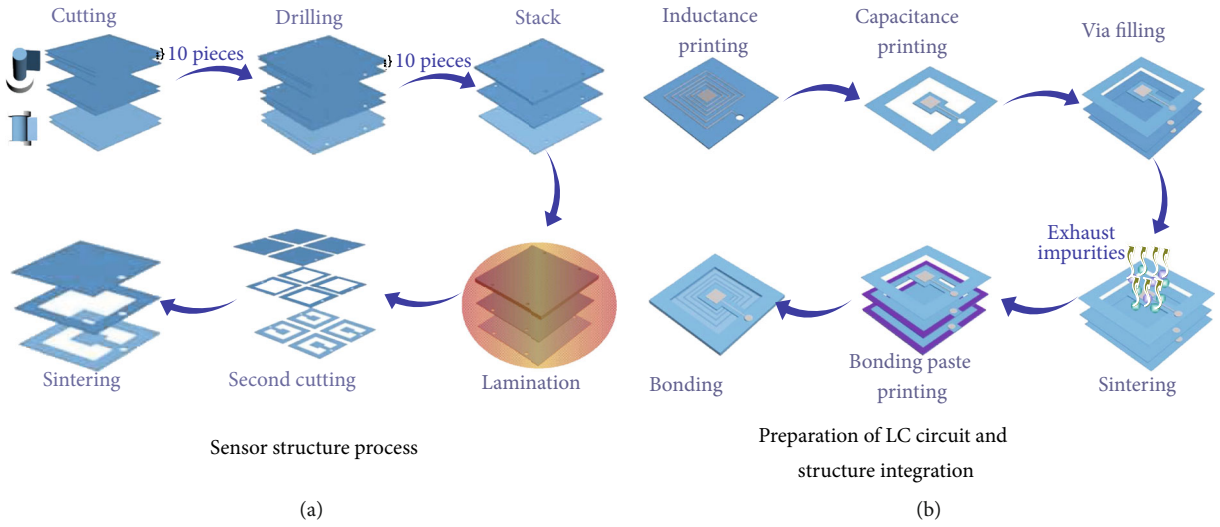

Figure 5: Fabrication process of the as-designed accelerometer: (a) fabrication of accelerometer structure; (b) preparation of LC series electrodes.

designed sensitive beam can be expected to work normally within 400°C.

4. Fabrication of LC Wireless Passive Vibration Sensor

In order to enable the sensor to work normally in high-temperature environment, the high-heat resistance ceramics are used as the materials of the vibration sensor. In addition, the bonding process is used to achieve the integrated manufacturing of the vibration sensor. The fabrication process mainly includes the processing of the sensor structure and the printing of the LC series electrodes.

4.1. Sensor Structure Process. Figure 5(a) shows the main preparation steps of the sensor structure process. In order to obtain a larger displacement of the sensitive beam mass under the same acceleration, zirconia ceramics with a low elastic modulus are used as the sensitive material in this study. First, the laser cutting technology is used to cut green ceramic tape into 14 pieces. Second, the laser drilling technology is used to punch through holes at designated via positions directly at 1 mm so as to fill the Ag paste to realize the interconnection between the capacitor and inductor. Then, the green tapes are stacked and laminated in 10 pieces, 2 pieces, and 2 pieces. After that, the laminated ceramic pieces are cut again using laser cutting technology to complete the structural dimensions of the frame, base, and beam mass. Finally, the cut sensor structures are sequentially placed into the muffle furnace for sintering. It is extremely important to set the holding time in the sintering process. If the holding time is too long or too short, it will have some impact on the sintered ceramic. The former makes the sintered ceramic soft and curved, while the latter makes the ceramic brittle. Different holding time leads to different changes in the properties of sintered ceramic sheets, so we optimize the sintering time by checking the performance of the ceramic sheet after

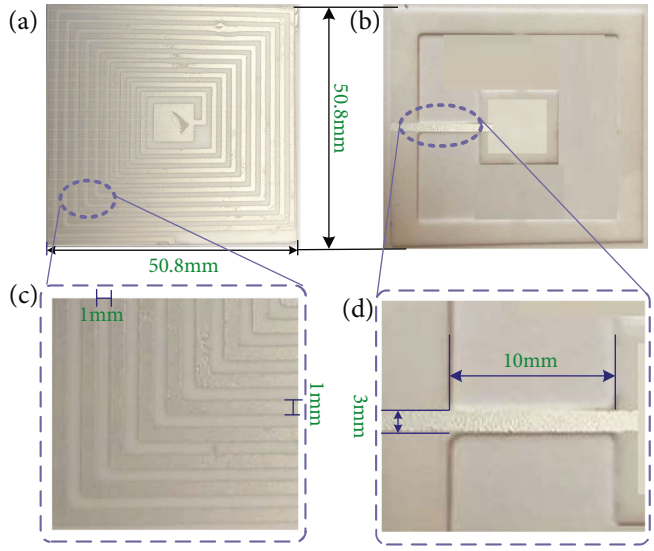

Figure 6: Fabricated sensor: (a) top surface of the vibration sensor; (b) sensitive beam of the vibration sensor; (c) partial view of the inductance; (d) partial view of the beam.

sintering. A large number of experiments show that it is suitable for holding time to set to 100 minutes, which not only can save time but also meet the characteristics of the material.

4.2. Preparation of LC Circuit and Structure Integration. The preparation process of the LC circuit and the integration of the structure are shown in Figure 5(b). In order to successfully achieve structural integration of the sensor based on different materials, screen printing technology and sintering technology are first used to prepare the LC circuit. Then, ceramic adhesives are used to realize the integrated preparation of the three-layer structure of the sensor. Conductive silver paste with low resistivity and excellent adhesion is used as

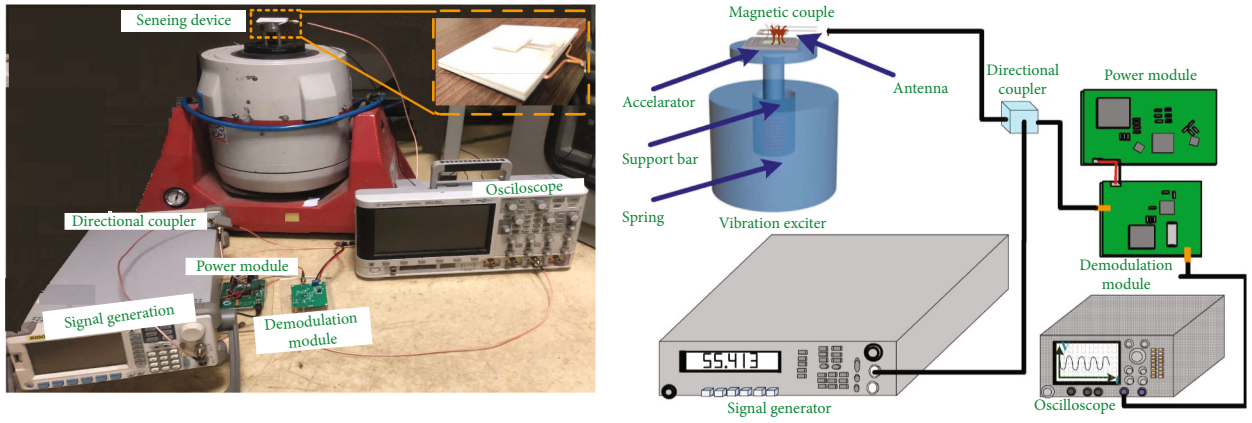

(a) (b)

Figure 7: Experimental platform of the vibration sensor: (a) diagram of the test platform built; (b) schematic diagram of the test platform.

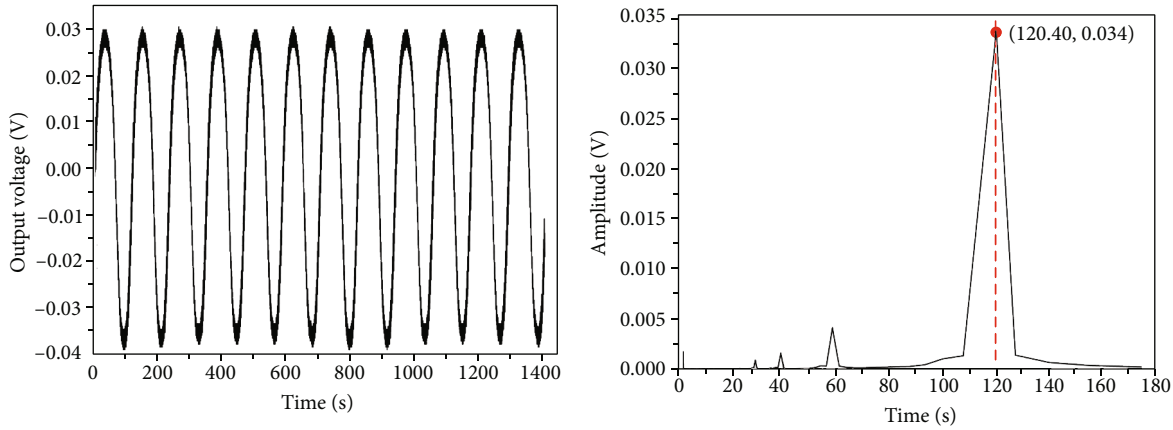

(a) (b)

Figure 8: The voltage output of the sensor under 120 Hz and 50 m/s^2 at room temperature: (a) waveform of output voltage; (b) fast Fourier transform spectrum of the waveform.

the LC circuit material. First, the ceramic surface is cleaned with alcohol and wipes to facilitate the adhesion between the slurry and high-temperature ceramics. Then, screen printing technology is used to allow the silver paste to uniformly pass through the customized screen plate so that the inductance and capacitance patterns are printed on the corresponding ceramic plate surface. Next, the silver paste is filled into the vias by the microhole filling machine to achieve the electrical connection of different layers. In addition, the frame, substrate, and beam-mass structure are placed in the muffle furnace for high-temperature sintering to remove impurities inside the slurry and achieve slurry purification. The peak temperature and holding time of sintering were 850°C and 40 min, respectively. Furthermore, ceramic bonding paste is printed on the sintered frame and substrate surface by screen printing technology. Finally, ceramic pieces printed with bonding paste are stacked together sequentially and placed in a muffle furnace for bonding at the maximum temperature of 600°C. The fabricated sensor is shown in Figure 6.

5. Measurement and Result

The experimental test platform was built for vibration measurement, as shown in Figure 7. The platform was mainly composed of a vibration exciter, a demodulation circuit (including a power supply module and a characteristic detection circuit module), an oscilloscope (general source DS6064), a signal generator (general source DG5252), and a directional coupler (ZEDC-10-2B). A standard vibration sensor was installed on the surface of the vibration exciter to detect whether the applied excitation changed sinusoidally. The sensor designed in this study was fixed on the exciter at a distance of 2 mm from the antenna, and a ceramic plate was used for insulation. The input and output ports of the directional coupler were connected to the readout antenna and the signal generator, and the third port, namely, the CPL port, was connected to the input port of the characteristic detection circuit. In addition, the output port of the characteristic detection circuit was connected to the oscilloscope. The signal source for the entire measurement system was

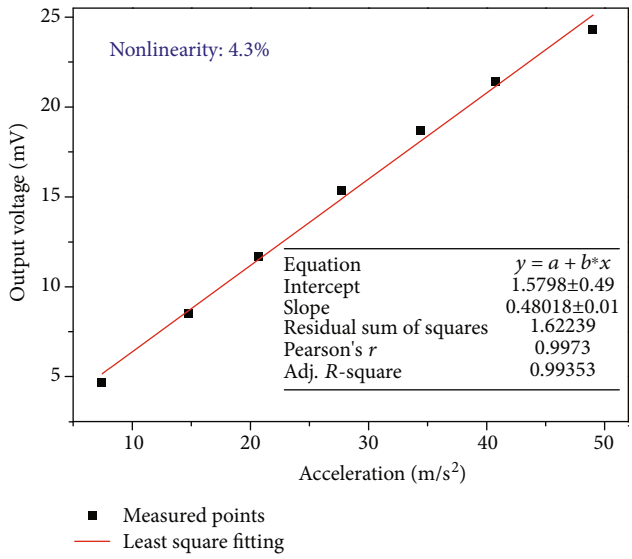

Figure 9: Voltage output as a function of acceleration at 120 Hz and room temperature.

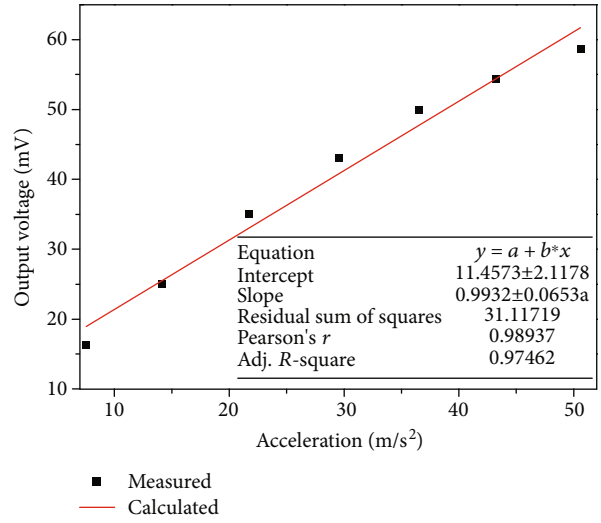

Figure 10: Sensor voltage output as a function of acceleration at 250°C.

provided by a signal generator. The reflected signal at the antenna was transmitted wirelessly to the CPL port due to impedance mismatch and was input to the detection circuit in the form of a sinusoidal voltage envelope through the directional coupler. The final sinusoidal voltage was detected and stored in the oscilloscope.

The continuous response waveform and frequency spectrum of the sensor at 120 Hz and 50 m/s^2 are shown in Figure 8. As shown in Figure 8(a), the sensor output voltage waveform changes sinusoidally with the excitation signal. By extracting the peak-to-peak value of the voltage waveform, the vibration sensitivity of the sensor is approximately 1.303 mv/m·s^{-2}. As shown in Figure 8(b), the frequency spectrum of the sensor was obtained through the fast Fourier transform analysis of the continuous response waveform. It could be seen that the vibration frequency was approximately 120.04 Hz, which was almost consistent with the excitation frequency set by the vibration platform.

In addition, we increased gradually the vibration acceleration from 4 m/s^2 to 50 m/s^2 at a normal temperature (25°C) and recorded the value of the output voltage to characterize the sensor performance. Because the test results included the noise in the detector circuit, Savitzky–Golay smoothing denoising processing was performed on the measured results before analysis to obtain more accurate results. The generated denoising output voltage as a function acceleration is shown in Figure 9. It could be seen that the output voltage amplitude increased with the increase of acceleration, and the nonlinear error was approximately 4.3% by least square fitting method, which indicated that the sensor has good linearity.

In order to further analyze the influence of temperature on sensor performance, we tested the performance of the sensor at 250°C. As shown in Figure 10, it was the relationship between the output voltage of the sensor and the acceleration at 250°C. We could see that the sensitivity of the sensor was 0.989 mv/m·s^{-2}, which was slightly lower than the sensitivity under normal temperature, and indicated that the sensor could measure vibration in high-temperature environment.

6. Conclusion

Based on the principle of mutual inductance coupling, an LC resonant sensor with acceleration sensitive structure is proposed in this paper. The vibration sensor sensitive structure is cantilever-mass structure. The measuring principle of the sensor is analyzed theoretically, and the mechanical properties of the sensitive structure are simulated under the field of acceleration and the coupling field of temperature-acceleration by ANSYS. The bonding process is used to fabricate the integration of the sensor with beam-mass structure successfully. The vibration sensor is tested by experimental platform built. It is proved that the sensor has good acceleration sensitivity and nonlinear error, which are 1.303 mv/m·s^{-2} and 4.3%, respectively. Moreover, the experiment at high temperature shows the sensor can measure the vibration within 250°C.

Data Availability

The experimental data used to support the findings of this study are included within the article.

Conflicts of Interest

The authors declare that they have no conflicts of interest.

References

[1] R. W. Johnson, J. L. Evans, P. Jacobsen, J. R. R. Thompson, and M. Christopher, "The changing automotive environment: high-temperature electronics," *IEEE Transactions on Electronics Packaging Manufacturing*, vol. 27, no. 3, pp. 164–176, 2004.

[2] W. C. Wilson and G. M. Atkinson, "Passive wireless sensor applications for NASA's extreme aeronautical environments," *IEEE Sensors Journal*, vol. 14, no. 11, pp. 3745–3753, 2014.

[3] A. Korashy, H. Attia, V. Thomson, and S. Oskooei, "Characterization of fretting wear of cobalt-based superalloys at high temperature for aero-engine combustor components," *Wear*, vol. 330-331, pp. 327–337, 2015.

[4] X. Men, F. Song, and H. Shao, "Investigation on transmission parameters of vibration measurement on high temperature environment," *Procedia Engineering*, vol. 15, pp. 5531–5535, 2011.

[5] S. Wang, X. Chen, C. Tong, and Z. Zhao, "Matching synchrosqueezing wavelet transform and application to aeroengine vibration monitoring," *IEEE Transactions on Instrumentation and Measurement*, vol. 66, no. 2, pp. 360–372, 2017.

[6] A. R. Sankar, J. G. Jency, and S. Das, "Design, fabrication and testing of a high performance silicon piezoresistive Z-axis accelerometer with proof mass-edge-aligned-flexures," *Microsystem Technologies*, vol. 18, no. 1, pp. 9–23, 2012.

[7] J. Wang, T. Wang, and H. Guo, "A new design of a piezoelectric triaxial micro-accelerometer," *Key Engineering Materials*, vol. 645-646, pp. 841–846, 2015.

[8] X. Zhou, L. Che, S. Liang, Y. Lin, X. Li, and Y. Wang, "Design and fabrication of a MEMS capacitive accelerometer with fully symmetrical double-sided H-shaped beam structure," *Microelectronic Engineering*, vol. 131, pp. 51–57, 2015.

[9] G. Radosavljevic, "Wireless LTCC sensors for monitoring of pressure, temperature and moisture," *Informacije MIDEM -. Journal of Microelectronics, Electronic Components and Materials*, vol. 42, pp. 272–281, 2012.

[10] M. Radovanovic, B. Mojic-Lante, K. Cvejin, V. Srdic, and G. Stojanovic, "A wireless LC sensor coated with Ba0.9Bi0.066-TiO3 for measuring temperature," *Sensors*, vol. 15, no. 5, pp. 11454–11464, 2015.

[11] P. Sturesson, Z. Khaji, S. Knaust, L. Klintberg, and G. Thornell, "Thermomechanical properties and performance of ceramic resonators for wireless pressure reading at high temperatures," *Journal of Micromechanics and Microengineering*, vol. 25, no. 9, article 095016, 2015.

[12] M. A. Martuza, C. Lee, A. Sazonov, S. Boumaiza, and K. S. Karim, "Wireless *LC*-type passive humidity sensor using large-area RF magnetron sputtered ZnO films," *IEEE Transactions on Electron Devices*, vol. 65, no. 8, pp. 3447–3453, 2018.

[13] Lei Dong, Li-Feng Wang, and Qing-An Huang, "Implementation of multiparameter monitoring by an *LC*-type passive wireless sensor through specific winding stacked inductors," *IEEE Internet of Things Journal*, vol. 2, no. 2, pp. 168–174, 2015.

[14] Q.-A. Huang, L. Dong, and L. F. Wang, "*LC* passive wireless sensors toward a wireless sensing platform: status, prospects, and challenges," *IEEE Journal of Microelectromechanical Systems*, vol. 25, no. 5, pp. 822–841, 2016.

[15] C. Zheng, W. Li, A. L. Li, Z. Zhan, L. Y. Wang, and D. H. Sun, "Design and manufacturing of a passive pressure sensor based on LC resonance," *Micromachines*, vol. 7, no. 5, p. 87, 2016.

[16] G. Zhang, Q. Tan, B. Lin, and J. Xiong, "A novel temperature and pressure measuring scheme based on LC sensor for ultra-high temperature environment," *IEEE Access*, vol. 7, pp. 162747–162755, 2019.

[17] T. Guo, T. Zhou, Q. Tan, Q. Guo, F. Lu, and J. Xiong, "A room-temperature CNT/Fe3O4 based passive wireless gas sensor," *Sensors*, vol. 18, no. 10, p. 3542, 2018.

[18] T. Wei, Q. Tan, T. Luo et al., "Modeling, simulation and coupling experiment for integrated passive wireless multi-parameters ceramic sensor," *Sensor Review*, vol. 36, no. 1, pp. 98–106, 2016.

[19] H. Liu, R. Fang, M. Miao et al., "Design, fabrication, and performance characterization of LTCC-based capacitive accelerometers," *Micromachines*, vol. 9, no. 3, p. 120, 2018.

[20] C. Li, Q. Tan, J. Xiong et al., "A noncontact wireless passive radio frequency (RF) resonant pressure sensor with optimized design for applications in high-temperature environments," *Measurement Science and Technology*, vol. 25, no. 7, article 075101, 2014.

[21] Y. Ji, Q. Tan, X. Lu, G. Zhang, W. Zhang, and J. Xiong, "Wireless passive separated LC temperature sensor based on high-temperature co-fired ceramic operating up to 1500 ˚C," *Journal of Micromechanics and Microengineering*, vol. 29, no. 3, article 035015, 2019.

[22] R. Nopper, R. Has, and L. Reindl, "A wireless sensor readout system—circuit concept, simulation, and accuracy," *IEEE Transactions on Instrumentation and Measurement*, vol. 60, no. 8, pp. 2976–2983, 2011.